Chemical Physics 541 (2021) 111018

Contents lists available at ScienceDirect

Chemical Physics

journal homepage: www.elsevier.com/locate/chemphys

Probing coupled motions of peptides in solution with fluorescence anisotropy and molecular dynamics simulation

Gouri S. Jas [a,*], Ed W. Childs [b], Krzysztof Kuczera [c]

[a] Department of Pharmaceutical Chemistry, The University of Kansas, Lawrence, KS 66047, United States
[b] Department of Surgery, Morehouse School of Medicine, Atlanta, GA 30310, United States
[c] Department of Chemistry and Department of Molecular Biosciences, The University of Kansas, Lawrence, KS 66045, United States

ARTICLE INFO

Keywords:
Fluorescence
Fluorescence lifetime
Molecular dynamics
Peptide
Order parameter
znisotropy

ABSTRACT

Here we present an atomically detailed study of local and global motions in two peptide systems, *N*-acetyl-tryptophanamide (NATA) and a pentapeptide WA_3K (WK5) combining detailed spectroscopic measurements and comprehensive computer simulations. We have measured fluorescence lifetimes, fluorescence anisotropy decay (FAD), far-UV circular dichroism (CD) spectra as a function of temperature, and carried out molecular dynamics (MD) simulation with an improved water model (TIP4P/EW). Fluorescence lifetime analysis showed the presence of a heterogeneous population of conformations in both peptides and a quenched fluorescence in WK5. Far-UV CD measurements quantified structural populations in both peptides specifying alpha-helix and sheet for NATA and 3_{10} helix and polyproline II for WK5 and their variation with temperature. FAD showed a bi-exponentiality in the reorientation dynamics, indicating the presence coupled motions in solution. The faster time constants, 6 ps for NATA, and 26 ps for WK5 are nearly temperature-independent and the slower components, 60 ps for NATA and 246 ps for WK5 at room temperature, vary with temperature. These faster and slower time constants are likely associated with the initiation and propagation steps of the reorientation dynamics. Results from MD simulation are in good agreement with the measured reorientation time and structural conformations. MD analysis showed that the measured faster time constants may be ascribed to delocalized molecular vibrations. Kinetic analysis found motions in the 1 ns in NATA and 10 ns in WK5. Both peptides exhibited markedly slower internal fluctuations compared to freely moving systems in the absence of overall translations and rotations, indicating a significant coupling between local and global dynamics. This study, focusing on simple model systems, has generated new insights into the dynamic behavior of peptides in solution.

1. Introduction

Biologically relevant molecules, like peptides and proteins, are inherently dynamic in their natural environment. The structural fluctuation of these biomolecules, both local and global, is determined to be an essential component [1–9] for their function like enzymatic reaction and signal transduction. Dissecting the dynamic components of peptide/protein motion and relating them to the structure remains challenging as they move away from the most populated state. There has been discussion about how internal and global motion, on the millisecond to second time-scale, might be coupled in a large protein molecule as it functions. Observing these motions in a much smaller system like di- and pentapeptides in solution requires a probe capable of capturing molecular events in the picosecond domain. It has been suggested that a direct coupling of motion would indicate that the size of a protein and the flexibility in its loops will significantly influence its function. It has also been inferred that protein dynamics is a combination of protein structural elements and the propagation of signal influencing the overall motion of protein [10–13]. It is not entirely clear how this applies to smaller systems where secondary structural elements are not readily present. It would thus be of fundamental importance to derive an atomically detailed picture of how these internal dynamics influence global motion in smaller systems.

In this study, we have measured temperature dependent fluorescence lifetimes, fluorescence anisotropy decay (FAD), and far-UV circular dichroism (CD) spectroscopy of two model peptide systems, NATA and WK5. CD data in a wide range of temperatures was introduced earlier in the preliminary form [14]. Here we have considered three temperatures

* Corresponding author.
E-mail address: gouri.jas@physicianscientists.org (G.S. Jas).

https://doi.org/10.1016/j.chemphys.2020.111018

relative to fluorescence lifetime measurements for structural quantification. A singular value decomposition (SVD) of the fluorescence lifetimes showed structural heterogeneities. Far-UV CD has characterized these heterogeneities. Temperature-dependent FAD identified two time-constants associated with the reorientation dynamics. The faster time constants are nearly temperature independent whereas the slower components are temperature dependent.

Molecular dynamics simulations have been carried out for NATA and WK5 with TIP4P/EW water model, a more realistic water system than our earlier work [14] with TIP4P. Structural sampling showed alpha-helical, turn, and extended state for NATA, and 3_{10} helical, turn, and extended conformations for WK5, as measured with CD. Reorientation time constants with TIP4P/EW [15] were 2 ps and 45 ps for NATA, and 33 ps and 170 ps for WK5, at room temperature. These results are in good agreement with the FAD and a significant improvement over the TIP4P results. Simulations further indicated that the faster time constant can be ascribed to delocalized molecular vibrations. We have generated additional MD trajectories in the absence of overall rotation and translation (NORT) for the peptides in solution to investigate the coupling between local and global motions. Here, the internal relaxation is found to be significantly slower compared to unrestricted MD (UNR), an important indication of a strong coupling between the local dynamics and rotational/translational motion. Kinetic analysis with Optimal Dimensionality Reduction (ODR) [16–17] and Markov State Models (MSM) [18], was also carried out for NATA and WK5. Kinetic result showed a relaxation rates of ca. 1 ns for NATA and ca. 10 ns for WK5.

Here we have shown that with carefully considered multiple rigorous experimental measurements, comprehensive molecular dynamics simulation and theoretical analysis can successfully identify and quantify heterogeneous structural populations, coupled internal and global motions, the origin and mechanism responsible for these motions, as well as structural relaxation rates and pathways of model peptide systems.

2. Methods

2.1. Materials

The Ac-Tryptophan-NH_2 (NATA) was procured from Sigma. The WK5, a five residues peptide, Ac-WA_3K-NH_2, was custom synthesized by GenScript Corporation with a greater than 98% purity. CD and FAD measurements on NATA and WK5 were carried in 20 mM acetate buffer at pH 4.8. Sample concentrations for NATA and WK5 were determined from the absorption spectra of each sample using the molar extinction coefficient of 5690 M^{-1} cm^{-1} at 280 nm.

2.2. Fluorescence anisotropy decay

Instrumentation is described in detail elsewhere [19]. Briefly, time-correlated single-photon counting was employed in time-resolved fluorescence measurements. NATA and WK5 fluorescence is generated with excitation at 290 nm, with the third-harmonic of a mode-locked, cavity-dumped Mira Optima 850F/Pulse Switch Ti:sapphire laser pumped by a 10 W Verdi Laser (Coherent, Inc., Santa Clara, CA, and 5–050 Ultrafast Harmonic Generator, Inrad Northvale, NJ) with an instrument response time between 5 and 10 ps. NATA and WK5 fluorescence was collected at 350 nm with an 8 nm bandpass (model 9030 monochromator, Sciencetech Inc., Concord, ON, Canada). The instrument response function collected with a dilute colloidal solution of nondairy creamer had a full width at half-maximum (FWHM) of ca 35 ps. This puts our fastest time constant of 6 ps near the instrument time resolution. A parallel and perpendicular fluorescence polarizations were collected simultaneously in a T-format and processed by a PC card (Becker and Hickl, SPC-830 detection efficiencies, a correction factor was incorporated into the fitting equations. The fitting parameter had a value g ≈ 0.5 where g is the relative detection efficiency of fluorescence with polarization perpendicular to the excitation polarization relative to fluorescence with polarization parallel to the excitation polarization. Fluorescence decays in parallel and perpendicular polarizations were globally fit to a two-exponential coupled to a double-exponential anisotropy decay.

2.3. Circular dichroism

Structural characterization with Far-UV CD spectroscopy at three different temperatures of NATA and WK5 in acetate buffer at pH 4.8 are measured on a JASCO 815 spectropolarimeter in a cylindrical cell with a path length of 0.5 mm and at a concentration of ~75 μM and 70 μM. Scans between 170 and 260 nm and 283 and 303 K were recorded at 10° interval. These peptide concentrations are significantly lower compared to our earlier work [20–25] in similar and much larger systems. In those studies, a concentration-dependent Far-UV CD failed to produce any noticeable change in the spectral features within the specified concentration. Therefore, aggregation is highly unlikely in the studied concentration level. To resolve overlapping spectral features a singular value decomposition (SVD) [26–28] was applied to the temperature-dependent spectroscopic signals – fluorescence intensity, far-UV CD spectra, and FAD, using MATLAB svd module. The SVD module in MATLAB-toolbox generates the matrix singular value decomposition (svd) where svd operates on matrix (X) and returns a vector with singular values. [U,S,V] = svd (X) creates a diagonal matrix S with same dimension as X , and a nonnegative diagonal elements in decreasing order, and unitary matrices U and V so that X = U*S*V'. SVD calculation involves finding the eigenvalues and eigenvectors of AA^T and A^TA. The eigenvectors of A^TA make up the columns of V, the eigenvectors of AA^T make up the columns of U. Also, the singular values in S are square roots of eigenvalues from AA^T or A^TA…. The singular values are always real numbers.

2.4. Computational

MD were performed for *N*-acetyl-tryptophanamide (NATA) and Ac-WA_3K-NH_2 (WK5) peptides in aqueous solution. For NATA we generated an unrestrained MD trajectory (UNR) of 200 ns with TIP4P-EW [15] water in a 32.9 Å cubic box. Analogously, a UNR of 5,000 ns was generated for WK5 with TIP4P-EW in a cubic box size of 40.4 Å. MD trajectories were also generated with overall peptide translations and rotations periodically removed (NORT) at every 20 fs of 200 ns length for NATA and 2,900 ns length for WK5. Details are summarized in the SI Tables S1 and S2. Initial peptide structures were generated with CHARMM [29] in the extended conformation for NATA and helical form for WK5. Solvation, addition of ions, energy minimization, NPT equilibration at 1 bar, and 300 K and NVT trajectory at 300 K were carried out with GROMACS version 4.5.6 and 5.1.4 [30], using the OPLS-AA protein force field [31]. The PME method was used to describe long-range electrostatic interactions [32], van der Waals interactions were truncated at 1.0 nm and all bonds were constrained with LINCS [33].

To describe system dynamics, autocorrelation functions (ACFs) were calculated for selected system variables. For axis reorientations, $C_1(t) = \langle \cos(\theta) \rangle$ is related to rotational diffusion rates [34], whereas $C_2(t) = \langle 3cos^2(\theta) - 1 \rangle/2$ is related to FAD decays [35], where θ is the axis reorientation during time t. For distance-type variables x, we use $C_1(t) = \langle \Delta x(t) \Delta x(0) \rangle$, with $\Delta x(t) = x(t) - \langle x \rangle$, while for angle-type variables ϕ, we use the circular statistics result $C_1(t) = \langle \cos(\phi - \langle \phi \rangle) \rangle$, with $\langle \phi \rangle$ as defined by Jammalamadaka et al [36]. Correlation times were obtained from these ACFs in two ways. Most simply, an average correlation time

corresponding to experimentally measured quantities, $C_2(t) = \langle 3cos^2(\theta) - 1 \rangle$ functions were calculated for the ^1L_b transition dipole axis or tryptophan, obtained as a combination of a and b in-plane vectors according to the description by Yamamoto et al. [37] In the simulations, we used ground-state parameters for the indole sidechain, although FAD experiments involve reorientation in the excited state. Since interactions with the environment might be different in the indole excited state, the MD results can provide only approximate models for the experimental data.

A synthetic description of peptide conformational dynamics was generated by building kinetic network models, using the ODR [15–16] and MSM [17] approaches. Details of these approaches have been described elsewhere [16]. Briefly, discretization of state space is performed by dihedral angle clustering and a set of transitions is generated based on MD trajectories. These are used to obtain the kinetic matrix **K** in ODR and transition matrix **T** in MSM. Kinetic coarse-graining is performed by PCCA+ [37] and the reduced rate matrix **R** is obtained as in. [38] MSM models are generated with Emma 1.4 [39]. Details of the kinetic models are presented in the SI.

3. Experimental results

3.1. Fluorescence lifetime

Shown in Fig. 1, fluorescence lifetime decay and resolved components with the application of singular value decomposition (SVD) of NATA and WK5 as a function of time at 283 K, 293 K, and 303 K. Fluorescence decays at three different temperatures are shown in Fig. 1A for NATA and in Fig. 1B for WK5. Fluorescence decays are progressively faster with increasing temperature. Details of tryptophan photo-physics in solution have been the topic of several previous studies [40–42]. At each of the studied temperatures, the fluorescence lifetime of WK5 is much faster than NATA, suggesting a quenching mechanism in the WK5 system. A possible source of this quenching is the interaction between protonated lysine and tryptophan. This provides an important structural information for WK5 in solution compared to NATA. SVD component analysis of the fluorescence lifetime for NATA and WK5 is shown in Fig. 1C and 1D, respectively. SVD application on the data matrix for temperature-dependent intensity decays for NATA and WK5 shows the presence of three significant singular vectors. Consequently, in the temperature-dependent fluorescence decay trajectory, three independent conformations can be ascribed to each component, like the presence of a dominant structural population and a disordered population as well as an intermediate population of structures. In an SVD analysis of

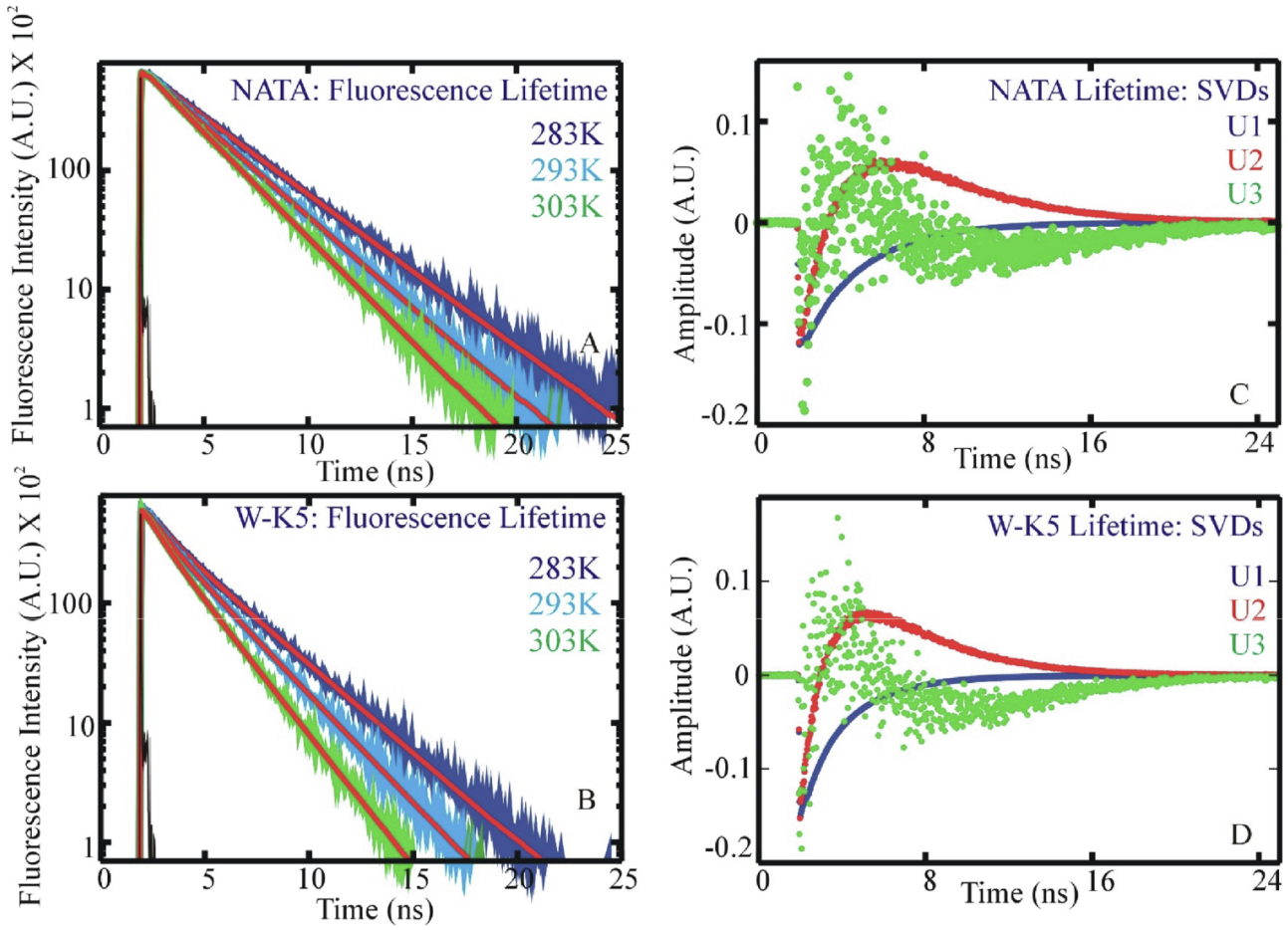

Fig. 1. Fluorescence Lifetime (FL) measurements and singular value decomposition (SVD) analysis of NATA and WK5 in solution. (A) Semi log plot with a bi-exponential fit to the fluorescence lifetime for NATA from 283 K to 303 K. FL data at 283 K, 293 K, and 303 K are in dark blue, light blue and green, respec-

time-resolved fluorescence trajectory as a function of increasing denaturant-induced unfolding of a protein, Laptenok et al. [43] resolved several structural components from their generalized approach to detecting folding intermediates from steady-state and time-resolved fluorescence. They assigned the resolved components to native, intermediate, and unfolded population states without quantifying the structural content. In a similar study, Kathuria et al. [44] applied SVD on the fluorescence lifetime data and resolved multiple overlapping features with different lifetimes where they attributed this finding to a local structural heterogeneity. Here we have used increasing temperature compared to previous study [43–44] to perturb the equilibrium and resolved overlapping structural population obtained with the application of SVD on the time-resolved fluorescence lifetime measurements to a specific population of structures employing far-UV CD.

A biexponential fit to the measured fluorescence lifetime with two resolved time constants is presented in Fig. 1A for NATA and 1B for WK5. The presence of a third time constant cannot be resolved with confidence as it is within the instrument time resolution of about 5 ps.

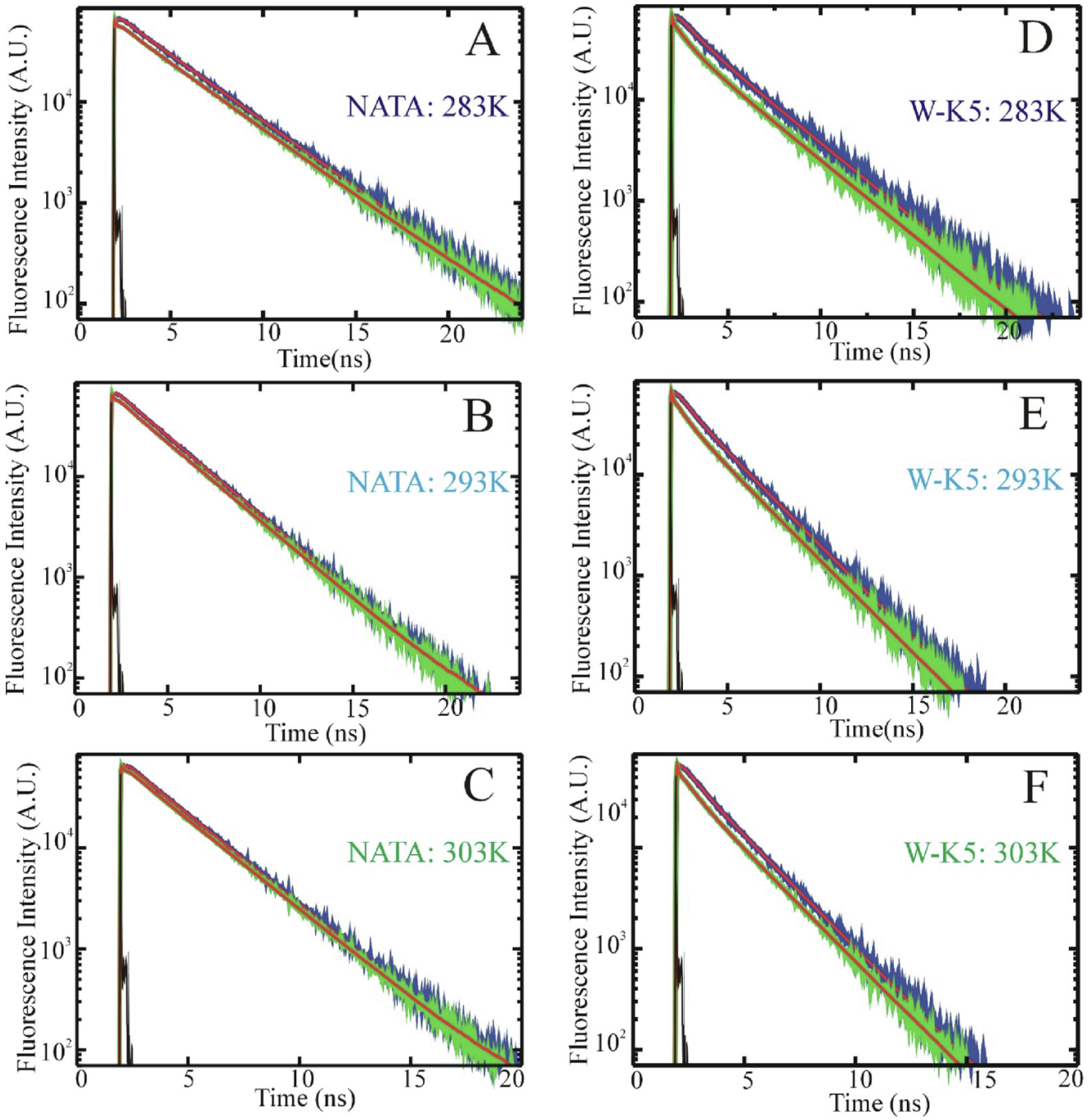

Fig. 2. Measured fluorescence decays (FD) in a semi-log plot employing time-correlated single-photon counting (TCSC) for NATA and WK5 in the parallel (blue) and

Two lifetimes at three different temperatures are generated for NATA with a bi-exponential fitting suggests the presence of two distinct structural populations. A third population of structures is present based on the SVD analysis and its lifetime is found to be significantly faster. Fluorescence lifetime for NATA at 283 K are measured to be 0.93 ± 0.06 ns and 3.34 ± 0.06 ns, 0.84 ± 0.04 ns and 2.82 ± 0.01 ns at 293 K, and 0.79 ± 0.05 ns and 2.45 ± 0.01 ns at 303 K, respectively. Fluorescence lifetime decay measurements at three different temperatures for WK5 are shown in Fig. 1B. Two lifetimes are generated with a bi-exponential fitting, suggesting the presence of two dominant structural populations for WK5. The lifetime of the third population is faster than instrument time-resolution. Fluorescence lifetime for these two states at 283 K are 0.85 ± 0.02 ns and 2.79 ± 0.08 ns, at 293 K 0.78 ± 0.02 ns and 2.35 ± 0.02 ns, at 303 K 0.69 ± 0.01 ns and 1.93 ± 0.01 ns, respectively.

3.2. Fluorescence anisotropy decay

Tryptophan fluorescence decay in parallel and perpendicular polarization are shown in Fig. 2, with NATA decays in Fig. 3A-C, and WK5 decays are in Fig. 3D-F. Fluorescence anisotropy decay of NATA and WK5 in three different temperatures are shown in Fig. 4. NATA FADs are in Fig. 4A-C. A bi-exponential fit produced two time-constants at each temperature with 6 ps and 94 ps at 283 K, 6 ps and 83 ps at 293 K, and 6 ps and 60 ps at 303 K. The measured faster time constant, around 6 ps for the simplest dipeptide NATA is resolvable but near the instrument time resolution. WK5 FADs are in Fig. 5D-F. Here the bi-exponential fits generate time constants of 29 ps and 328 ps at 283 K, 28 ps, and 298 ps at 293 K, and 26 ps and 247 ps at 303 K. For both peptides, the longer reorientation times become significantly faster with increasing temperature, while the faster time constants are essentially temperature independent.

A comparison of single- and double-exponential fits to FAD signals is shown in the SI, Figure S3. This clearly shows that the single-exponential function is unable to describe the measured data without missing the initial fast components. A bi-exponential function fully describes the measured decay curve, supporting the presence of processes on two time-constants in both NATA and WK5.

The observation of a fast temperature-independent and a slower temperature-dependent process in the FAD may be explained by the presence of a coupled motion. Here the initial process is an initiation step in the form of an internal motion through vibration. It may then propagate to trigger a global reorientation motion. The initiation process starts with the vibrational motion upon excitation of the tryptophan indole ring with 280 nm photons which propagates and manifests into a global reorientation motion. It appears that the initiation process is nearly temperature independent. The slower components of the reorientation time for NATA is observed to be about three times faster than WK5. These findings point to a size and shape differences in two systems in an identical solution condition. This is a reasonable assessment considering the smaller hydrodynamic volume and compactness of NATA.

Shown in Fig. 5 is the application of SVD on the data matrix of temperature-dependent FAD of NATA and WK5. For NATA (Fig. 5A) we see a decrease in amplitude in V1 with a concomitant increase in V2 and

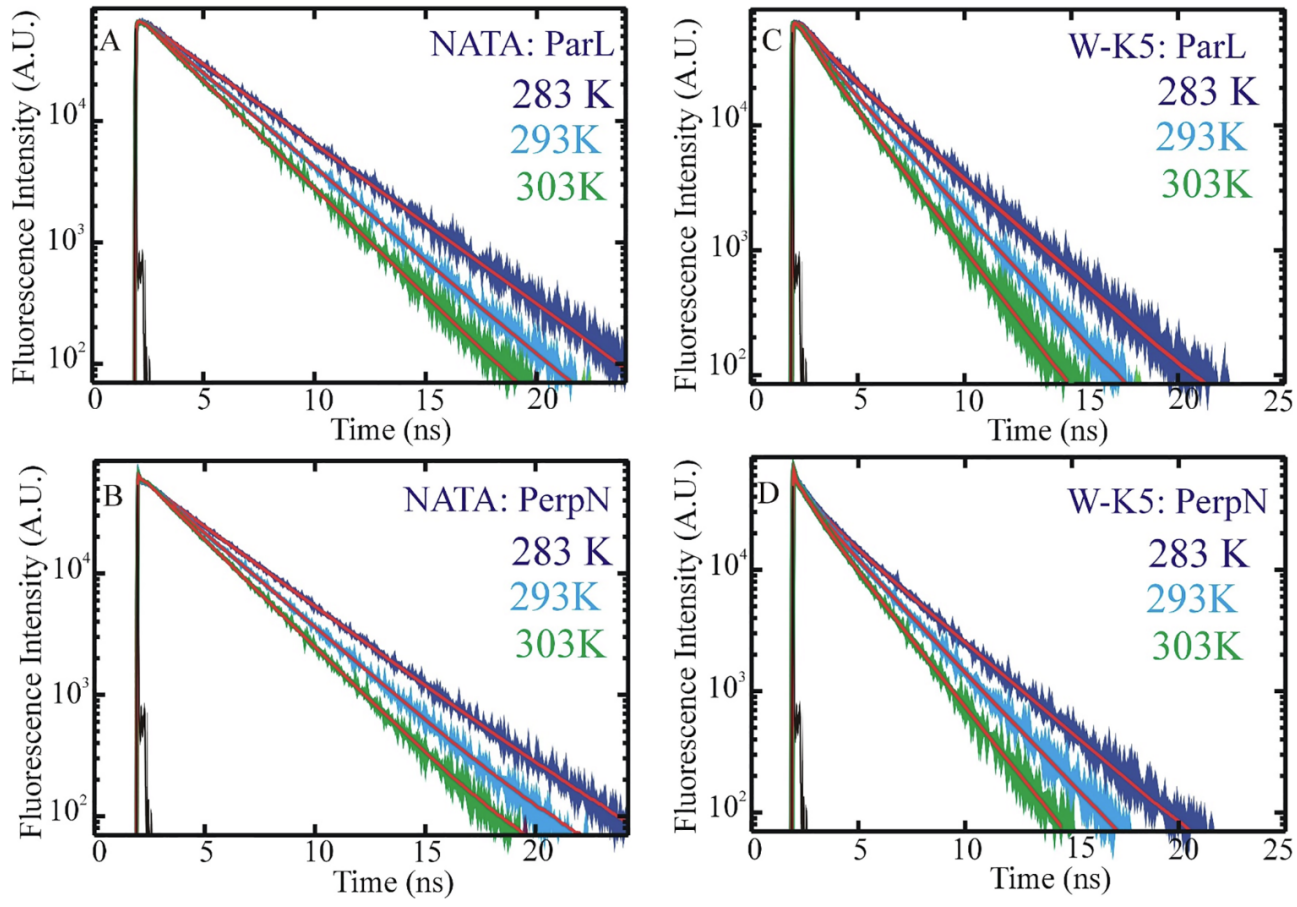

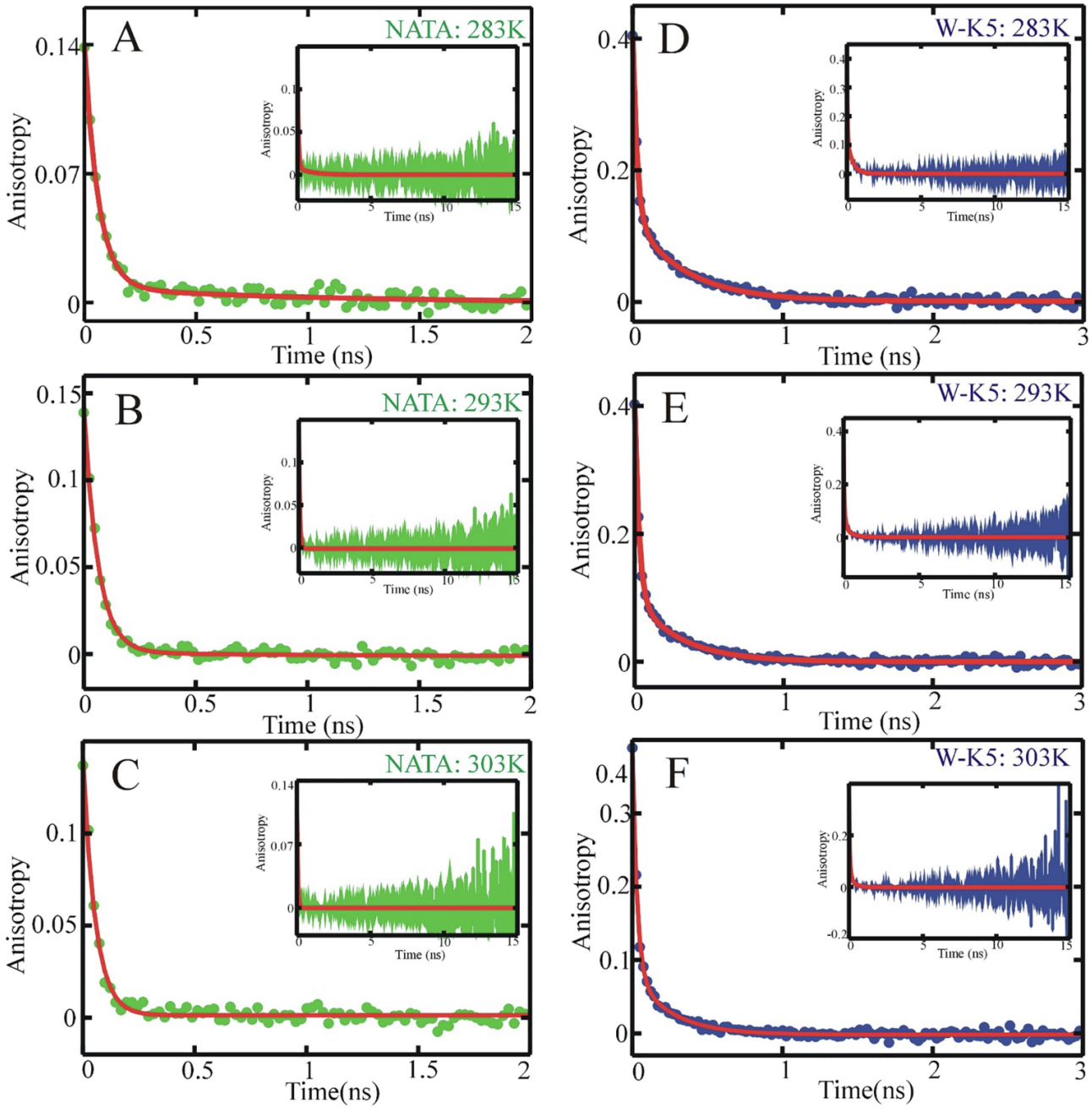

Fig. 4. FAD (fluorescence anisotropy decay) for NATA and WK5 from 283 K to 303 K. FAD for NATA from 283 to 303 K is shown in (A), (B), and (C), respectively with inset showing the entire measured data. For WK5, measured FAD from 283 to 303 K are shown in (D), (E), and (F), respectively with the inset showing the entire data with fit.

a small increase in amplitude in V3. A global fit to these vectors produced time constants that are very similar to the time constants observed from fitting the FAD data. Slower time constants for V1, V2, V3 for NATA are 58 ps, 65 ps, and 61 ps, respectively. The faster times constants are about 7 ps. For WK5 (Fig. 5B) a bi-exponential fit to V1, V2, and V3 are 29 ps and 256 ps, 28 ps and 303 ps, 28 ps, and 333 ps, respectively. Fluorescence lifetime analysis provides us with a picture of the possible population of states in the solution and their corresponding lifetime. FAD analysis with SVD directs us to view the reorientation dynamics of theses population and how these motions may be coupled of the studied system is consistent with the procedure carried out by Kathuria et al. [44]. Similar to the observation made in this report, Kathuria et al. described that their kinetic analysis is consistent with the lifetime analysis where the depopulation of the first state leads to the concomitant increase in the population of a second state. Like our analysis, their finds of positive amplitude vector V1 and negative amplitude for vector V2 are consistent with their kinetic analysis. Here, our observation of a negative and positive amplitude in the FAD with SVD may further attribute the presence of a motion that is couple during its reorientation dynamics

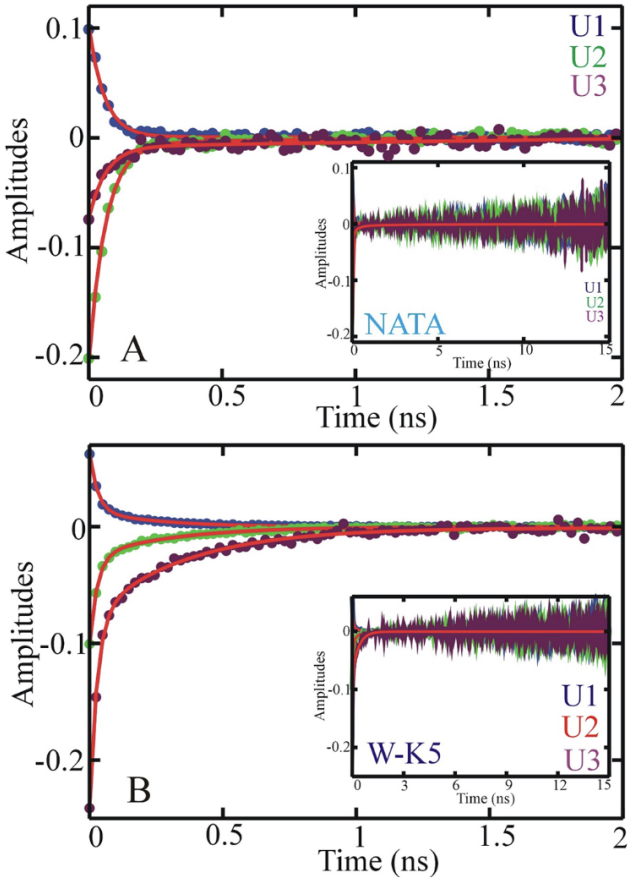

Fig. 5. Singular value decomposition (SVD) of the temperature-dependent raw FAD data. For NATA, the first three basis vectors, V1, V2, V2 with bi-exponential fit (red) are shown in (A) with inset showing the entire data with the fit (red) from FAD measurement. The first three basis vectors with the bi-exponential fit (red) for WK5 are shown in (B) with inset showing the entire FAD data with fit.

3.3. Circular dichroism

To quantify heterogeneous structural elements from the fluorescence lifetime analysis, we employed a Far-UV CD. Fig. 6 presents far-UV CD spectra of NATA and WK5. CD spectra at three different temperatures explored the structural population from FAD. For NATA (Fig. 6A) there are two minima at 198 and 210 nm and two maxima at 185 and 225 nm, pointing to an ordered structural population that changes with changing temperature. The components (U1, U2, U3) for NATA, obtained with SVD [19–24,45–47] are shown in Fig. 6B. The corresponding amplitude vectors, or weights, (Sv1, Sv2, Sv3) with respect to temperature are presented in Fig. 6B in-set.

CD spectra of WK5 between 283 K and 303 K are presented in Fig. 6C. Spectral features show that there are maxima at 227 and 185 nm and a minimum at 198 nm. An isodichroic point is located near 207 nm. The presence of a significant amplitude is also observed at 220 nm in the temperature-dependent spectra, which is commonly found in a helical conformation. Spectral component analysis for WK5 with SVD is shown in Fig. 6D. The three component spectra have a classic signature of a helix and coil state. The inset of Fig. 6D shows amplitude vectors (Sv1, Sv2, Sv3), as a function of temperature.

CD analysis for NATA and WK5 showed a significant population of ordered structure like a helix, hairpin, and coiled like state is present. It analysis. This is a helix-like conformation more like 3_{10} helical conformation. The U2 component shows a minimum of 220 and a maximum at 190 nm. Model CD spectra [48] suggests this may contain an appreciable population of helical state.

SVD of WK5 shows a maximum at 225 nm with a minimum at 200 nm in U1. This is like a poly-L-proline II. The U2 component shows a small minimum at 235 nm and a pronounced minimum at 212 nm with a maximum at 192 nm. This resembles a model hairpin-like conformation. The U3 component is found to be noisy with no significantly appreciable features.

DichroWeb [48] analysis of the measured CD spectra for NATA and WK5 was performed to characterize the structures and was found to be consistent with SVD component analysis. A helix, beta-strand, turn, and unordered structures were found for NATA. A 3_{10} helix, polyproline II, turn, beta, and unordered forms were sampled for WK5. The structural populations exhibited small shifts with a change in temperature. A detailed description is provided in the SI.

It is particularly significant that in a small pentapeptide like WK5 there exists an appreciable amount of 3_{10} helical population of structures which is rarely observed. The dynamic study is equally important, as the observed behavior in dynamics will include elements specific to these populations of structures.

These experimental findings require an atomically detailed description to develop a microscopic understanding involving the mechanism of these processes. To fully describe measured observables, we have employed an all-atom molecular dynamics (MD) simulation for both NATA and WK5 in solution at 300 K. The primary objective is not only to reproduce experimental observables computationally, but also to determine the molecular mechanisms like conformational equilibria, dynamical timescales, and coupled motion.

3.4. Computational results

Here we have carried out a comprehensive computational study with all-atom molecular dynamics simulations in explicit solvent. Using the MD trajectories, we have modeled the structural populations, internal and global dynamics, and solute–solvent interactions of the two peptide systems. In this simulation study, we have used TIP4P/EW as the viscosity of TIP4P/EW is much closer to the experimental value compared to the TIP4P that we applied earlier [14]. To analyze the coupling between local and global motion, we have followed the effects on the internal dynamics by removing peptide translation and rotation (NORT trajectories). As a result of the applied frequent system adjustments, the NORT trajectories do not represent realistic peptide dynamics. They primarily show the qualitative effects of global motion removal. More details are presented in SI.

3.5. Sampled structures

Representative molecular structures sampled with TIP4P/EW [15] for NATA and WK5 are presented in Fig. 7. For NATA they are mostly turn-like, as well as α, β, and polyproline II (PPII) backbone conformations. In WK5, they are mostly coil sates, with minor contributions from bend, turn, and 3_{10} helix. In both peptides, structures sampled in TIP4P/EW show a similarity with those seen in TIP4P water [49]. Our predicted structural populations qualitatively agree with the experimental observation from Far-UV CD results: helix, beta, and turn (no PPII) for NATA and 3_{10} helices, PPII, turn and unordered for WK5. A more detailed description is presented in the SI. Fig. 8.

3.6. Dynamical time scales

Dynamical time scales of the peptide motions were obtained by

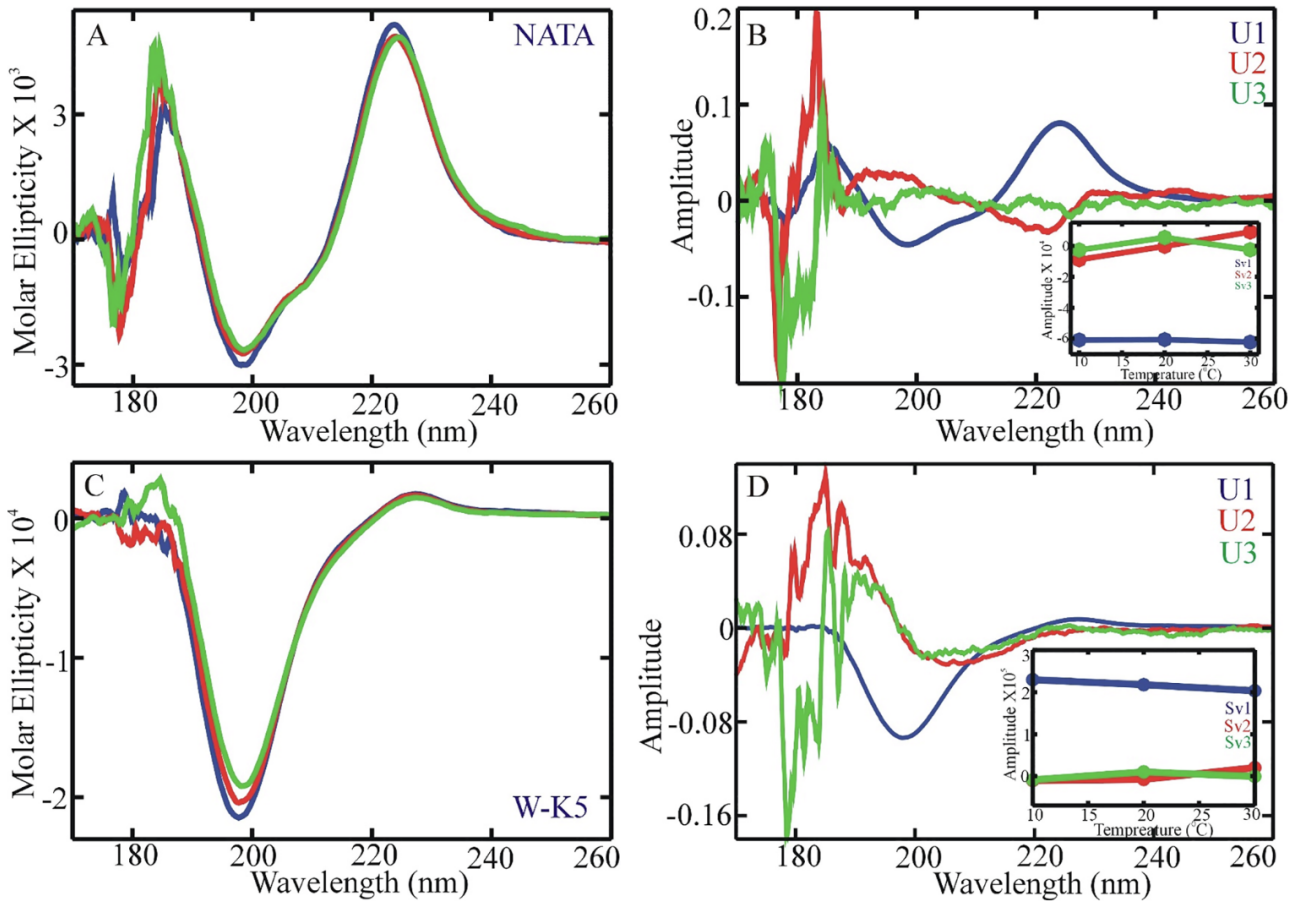

Fig. 6. Far-UV circular dichroism (CD) measurements with singular value decomposition (SVD) for NATA and WK5. (A) NATA far UV CD from 283 to 303 K. (B) The first three basis vector U1, U2, U3 (blue, red, and green) of NATA temperature-dependent CD with inset showing amplitude vectors of the first three components (blue, red, green) with respect to temperature. (C) WK5 Far-UV CD from 283 to 303 K. (D First three basis vector U1, U2, U3 (blue, red, and green) of WK5 temperature-dependent CD with inset showing amplitude vectors of the first three components (blue, red, green) with respect to temperature.

from starting structure (RMSD), and local variables like individual backbone (ϕ, ψ) dihedrals and sidechain dihedrals. The main results are summarized below, with details provided in the SI.

In the simplest picture, we look at the average relaxation times given by integrals under the ACF curves. These fall in the 40–420 ps range for NATA and 2.9–4.6 ns for WK5 and are comparable to those found in the earlier work [14] with TIP4P. The slowest decays are found with the RMSD variable and the Trp-$\chi_1$sidechain dihedral for both peptides. Looking at the ACFs in more detail, the simulation data may be well represented by three-exponential fits, corresponding to ultrafast, fast, and slower processes. For NATA associated time scales for these components are 0.3–0.7 ps, 5–18 ps, and 40–750 ps, while for WK5 they are 0.3–0.8 ps, 13–72 ps, and 160–3600 ps. Representative ACFs are shown in Fig. 9 and in SI.

Based on oscillatory motions present in the time courses of the underlying dynamical variables and the range of associated time constants, the two fastest components may be assigned to vibrations. The ultrafast motions would then correspond to more localized vibrations of frequency 50–100 cm^{-1} in both peptides, most commonly representing dihedral angle fluctuations around equilibrium values [50]. The fast motions would be due to delocalized vibrations of 2–6 cm^{-1} for NATA or 2 cm^{-1} or lower frequency for WK5, such as breathing modes [51]. Normal mode analysis in the gas phase applying CHARMM [29], yields the lowest frequencies for extended conformer of NATA of 27 cm^{-1}. For frequencies lower than those predicted by vacuum normal mode analysis [52–53]. Thus, the lowest vacuum vibrational frequencies for the two peptides qualitatively agree with the fast processes identified in the MD. The rationale behind assigning the ultrafast dynamical process to the delocalized vibrations is that the associated time scales are found to be qualitatively identical from the trajectory analysis considering many different reaction coordinates for each peptide system. In the experimental data, the corresponding time scales are temperature independent, suggesting that the underlying motions are not influenced by temperature-related solvent viscosity changes, supporting the vibrational assignment. The slower processes identified in the MD trajectories may be assigned to internal fluctuations and reorientation dynamics. Here we see a wide variation of time scales for different variables.

3.7. Modeling reorientations

To model molecular reorientation dynamics and compare it with the FAD, we have identified two ACFs generated from the MD trajectory. The ACF C_2(t) following the ^1L_b axis of the indole ring in tryptophan sidechain is used to compare with the measured FAD. The ACF C_2(t) for the reorientations of the end-to-end vector is related to global motion. Here, these functions are directly compared with the FAD at room temperature, shown in Fig. 7. A bi-exponential fit to the ACFs is found to be essential to adequately describe the entire function. Associated time

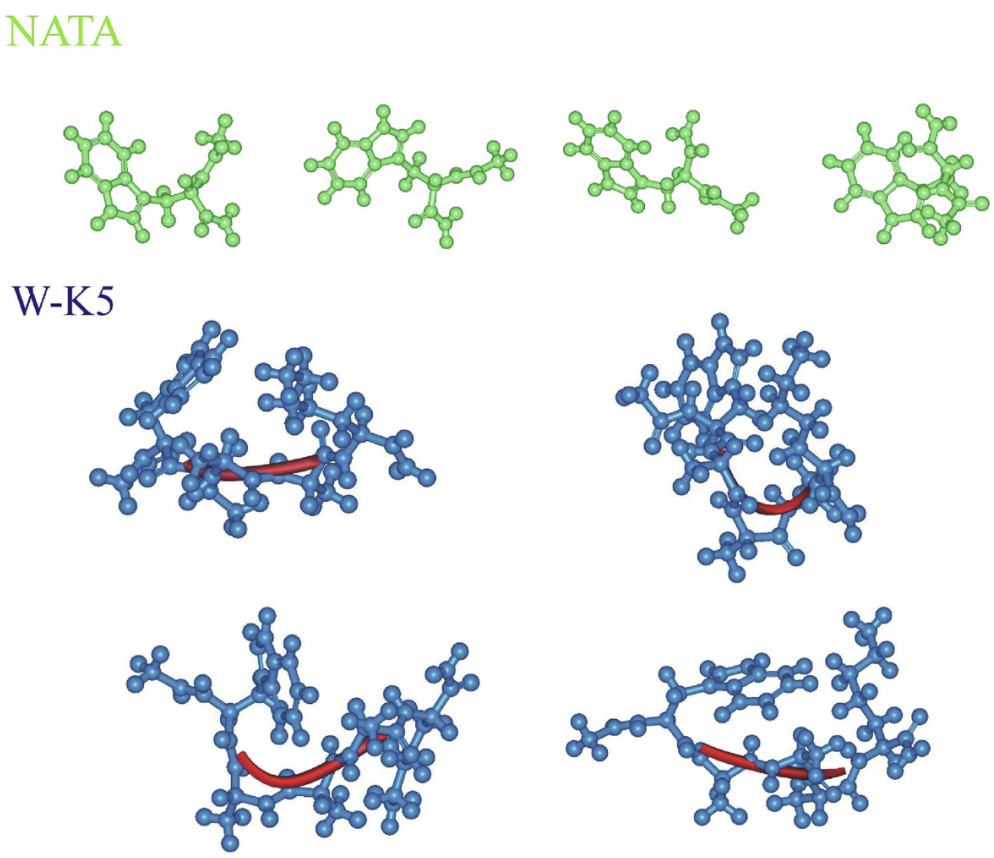

Fig. 7. Sample structures of NATA and WK5 from TIP4P/EW molecular dynamics simulations at 300 K.

vector reorientation axis at room temperature. For WK5, a time constant of 33 ps and 170 ps for ^1L_b axis and 50 ps and 250 ps for the end-to-end vector axis are obtained from MD trajectory analysis. The experimental time constants from FAD are 6 ps and 60 ps for NATA and 26 ps and 247 ps for WK5 at room temperature. The faster ^1L_b axis MD time constant in WK5 is comparable to the corresponding FAD result, while for NATA it is 1 ps, falls within the instrument time resolution. Faster time scale both systems fall in the time scales related to delocalized vibrations of the peptides. The slower computed transition dipole reorientations are found to be systematically below the measured data, by a factor of 25–50%. This may partly be explained due to the 8% underestimation of water viscosity in TIP4P [49] compared to TIP4P/EW [15]. We expect MD results to provide only approximate models for the observations, in general, due to the simplified nature of the water and protein force fields and specifically due to using the ground state Trp parameters for FAD simulations. Interestingly, the global reorientation dynamics represented with the end-to-end vector are found to be slightly slower in NATA and significantly slower in WK5 compared to the transition dipole motion along the indole ^1L_b axis.

3.8. Coupling of internal and global motions

Analysis of NORT MD trajectories is shown in Fig. 9. More results from this analysis are presented in the SI. Examples of effects include RMSD fluctuation rates falling by a factor of 3 in NATA and 2 in WK5, and Trp φ dihedral fluctuation rates decreasing by a factor of 3 in NATA and 5 in WK5. These results show significant slowing down of peptide reorientations as well as of internal fluctuations when global motions are

In our earlier analysis [14] of MD trajectories, we have applied a clustering approach with TIP4P water to determine major conformers, the dynamic elements, and performed reorientation with dihedral-restrained simulations (DRS) of the cluster center structure to obtain models to specify contributions to the overall FAD data. These trajectories explored peptide motions where global translation and rotation were allowed, but conformational transitions were removed due to the dihedral restraints. This was the opposite effect of that studied here, where we use NORT trajectories, in which only internal dynamics were possible. Internally rigid conformers of WK5 exhibited reorientations that were significantly slower compared to a freely fluctuating system, whereas in NATA internal rigidity had very little influence on rotational diffusion. Therefore, NORT suggests that the presence of overall translations and rotations is essential for internal fluctuations in both peptide systems. The coupling between global and internal motions may thus be asymmetric in NATA as removal of internal fluctuations did not influence reorientation time, but the elimination of global translations and rotations slowed down internal fluctuations.

3.8.1. Order parameters

Order parameters, S^2, are used for characterizing local protein dynamics and comparing simulations with experiments. Here we have derived order parameters for NATA and WK5 to examine the local peptide motion in solution. The main-chain Lipari-Szabo [54] order parameter (S^2) was derived from UNR and NORT simulations for NATA and WK5 (shown in the SI). In NATA there is a small difference in the order parameters between the UNR and NORT. This may be due to the greater role of localized motions in NATA dynamics. For WK5 our analysis shows a small difference in the order parameters between UNR

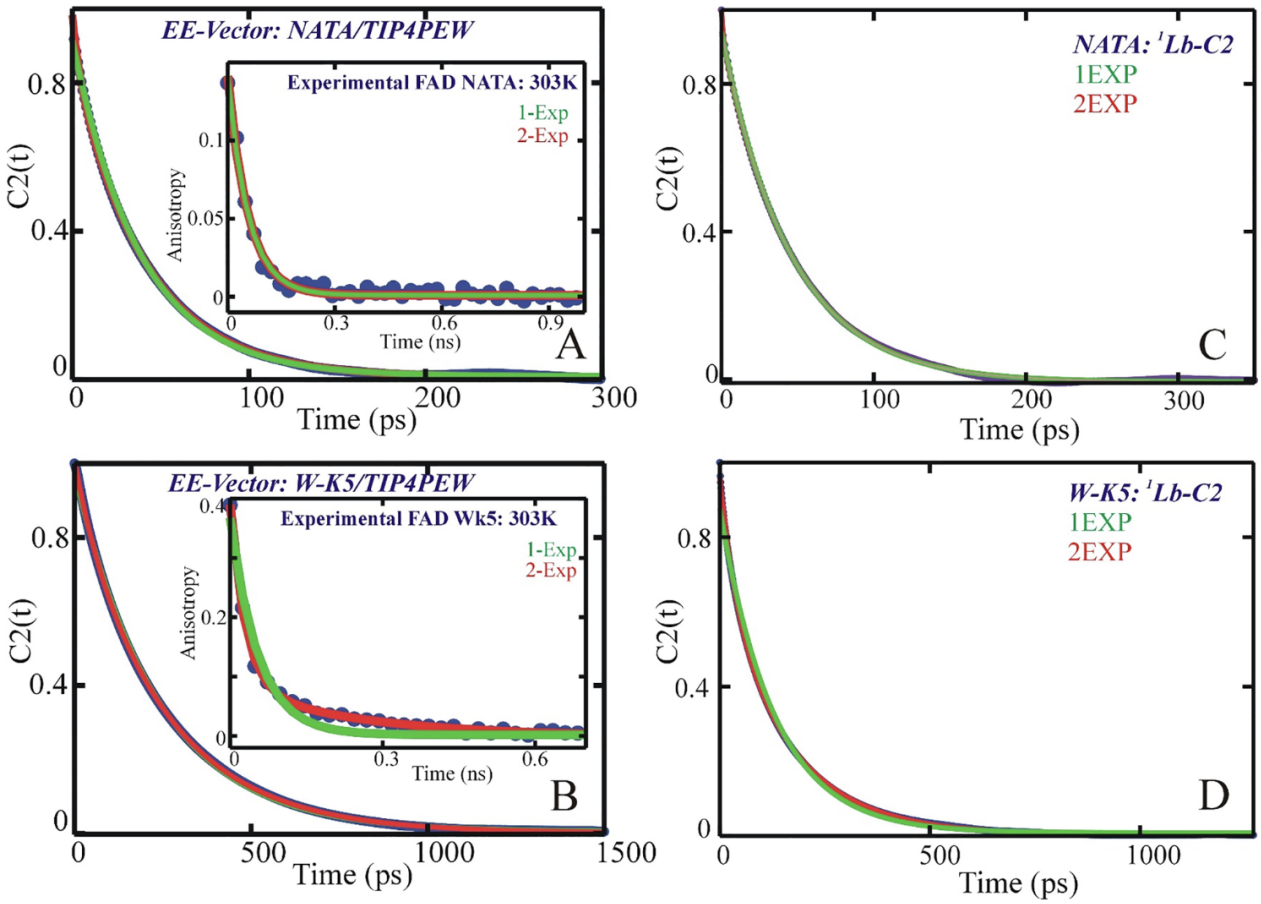

Fig. 8. MD in TIP4P/EW at 300 K: (A) NATA C_2 ACF of the end-to-end vector reorientation (inset: experimental FAD signal) (B) WK5 C_2 ACF of the end-to-end vector reorientation (inset: experimental FAD signal) (C) NATA C_2 ACF of the ^1L_b transition dipole vector reorientation. (D) WK5 C_2 ACF of the ^1L_b transition dipole vector reorientation. Single-exponential fits shown in green, two-exponential fits in red.

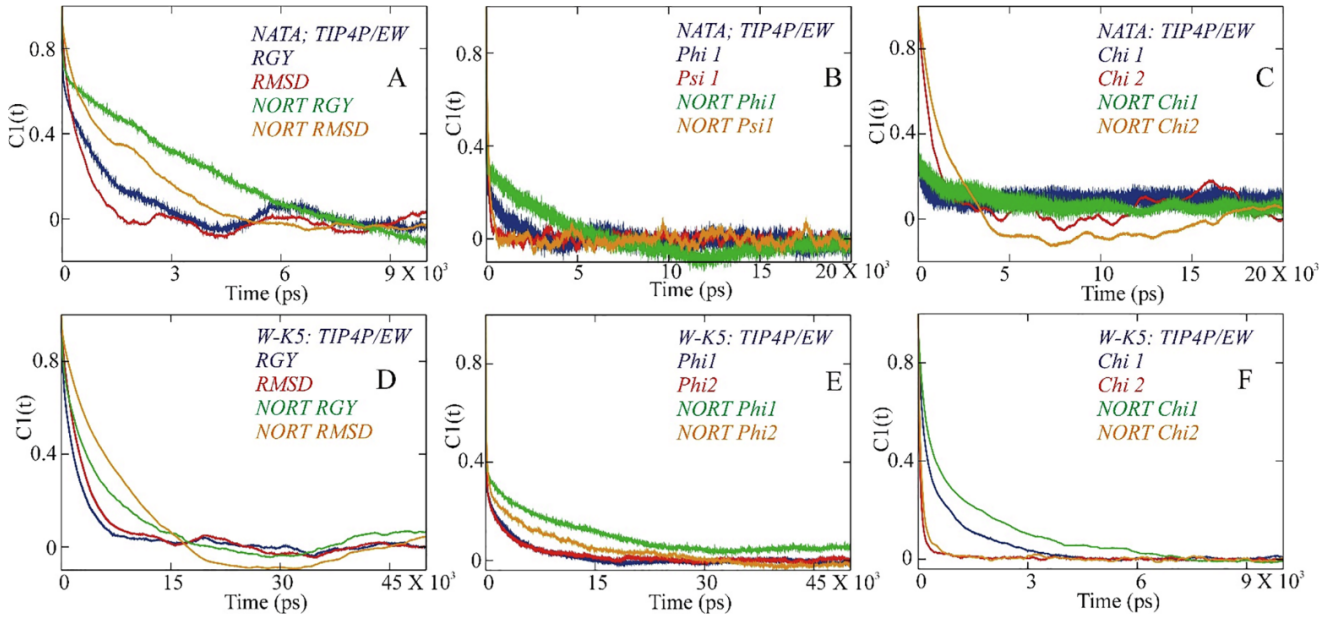

Fig. 9. Examples of C_1 ACFs of dynamical variables in MD of NATA (A-C) and WK5 (B-D) at 300 K in TIP4P/EW. Results from regular and NORT trajectories are

-C termini of WK5, which are more flexible and involved in delocalized dynamics, exhibit stronger coupling between internal and global motion. This observation is consistent with our C_2-autocorrelation function analysis. Hamaneh et al. [55] in their study of order parameters for a small globular protein to examine the presence of a coupling between internal and global motion found a small, nonsystematic difference in S^2 and the C_2-autocorrelation function for the residues. Based on the analysis, they found that global motion has a negligible effect on the order parameter. In contrast, our analysis found differences in the S^2 and $C_2(t)$, suggesting the presence of a coupled motion in the peptide systems.

3.8.2. Solute-solvent interactions

Solute-solvent interaction is an integral component in the reorientation dynamics of biomolecules in solution. Microscopic analysis of solute–solvent interactions was carried out by examining radial distribution functions (RDF), solvent accessible surface area (SASA), hydrogen bond dynamics, and energy fluctuations. Analysis of hydrogen bond dynamics used the approach described by Luzar-Chandler[56], and results are shown in the SI section. Employing TIP4P/EW [15] the peptide-water hydrogen bond correlation times τ_{HB} obtained with the Luzar-Chandler method were 5.9 ps for NATA and 9.3 ps for WK5; water-water interaction times were 5.1 ps for both peptides.

In Fig. 10 we have described the dynamics of the solute–solvent interactions of NATA and WK5 in TIP4P/EW by examining the RDF between peptide atom groups and water oxygens (OWT). Shown in Fig. 10A, is a stronger interaction between NATA carbonyl (C═O) and OWT compared to WK5. Interactions of OWT with backbone nitrogen (Fig. 10B), and indole group (Fig. 10C) exhibited similar trends for NATA and WK5, as observed between C═O and OWT. This suggests that WK5 is less exposed than NATA to the water. Residue by residue C═O interaction with water for WK5 revealed that Ala2, Ala3, and Ala4 are located in the more compact region of the peptide, with less solvent exposure, to *N*-terminal acetyl group and Lysine, the fifth residue, presented in Fig. 10D. The positively charged Lysine sidechain NZ atom exhibited a very strong interaction with water, almost identical to OWT-OWT interaction. This shows the presence of a well-defined water solvation shell for Lysine NZ, presented in Fig. 10E. Backbone beta-carbons (Cb) for Ala2, Ala3, and Ala4 interact with OWT with almost identical propensity whereas the Cb for lysine is less exposed to water and presumably interacting more with the peptide, presented in Fig. 10F. Overall this analysis presents an atomic-level description of the solution structure and the effect of an immediate aqueous environment for NATA and WK5. This may play an important role in our reorientation dynamics study specifying the most probable interaction during the global reorientation motion in the studied systems.

SASA averages and fluctuations in TIP4P/EW water are described in the SI. The C_1 ACFs of SASA fluctuations exhibit a sub-picosecond and ~ 1 ns component for NATA and 0.5 ns and 10 ns components for WK5. The van der Waals interactions of the peptides with solvent are presented in more detail in the SI section. In NATA, the major contributions correspond to the sub-picosecond motions ascribed to localized vibrations and a ~ 1 ns time related to the slowest kinetics of the indole sidechain rotation. In WK5 the fast component is in the hundreds of picoseconds, in the range of local internal fluctuations, and a 10 ns component representing the slowest dynamical mode may be related to the folding of the 3_{10} helix.

3.9. Kinetic models

Kinetic models using both ORD and MSM formalisms were generated for the two studied peptides. A more detailed explanation is provided in the SI. For NATA, a clear picture emerges of the slowest dynamical processes involving transitions between different conformers in the sidechain χ_1 (g-, g+, and t) and χ_2(a and s) dihedrals. The ORD and MSM models agree with respect to time scales and types of transitions. The slowest motions involve χ_1 transitions on 1.0–1.5 ns time scale and these relaxations are well separated in time from the rest. Presented in Fig. 11 is an example of a kinetic analysis for NATA, employing trajectory discretization with $N_c = 8$ dihedral clusters with three coarse-grained states, showing χ_1 transitions on the nano/sub-nanosecond time scale and χ_2 transitions.

For WK5, the kinetic result is more complex. Individual residues of WK5 tend to sample four main backbone conformers – turn, extended, PPII, and 3_{10} helix. In TIP4P/EW simulations the slowest motions involve transitions between extended/PPII and turn/3_{10} helix structures

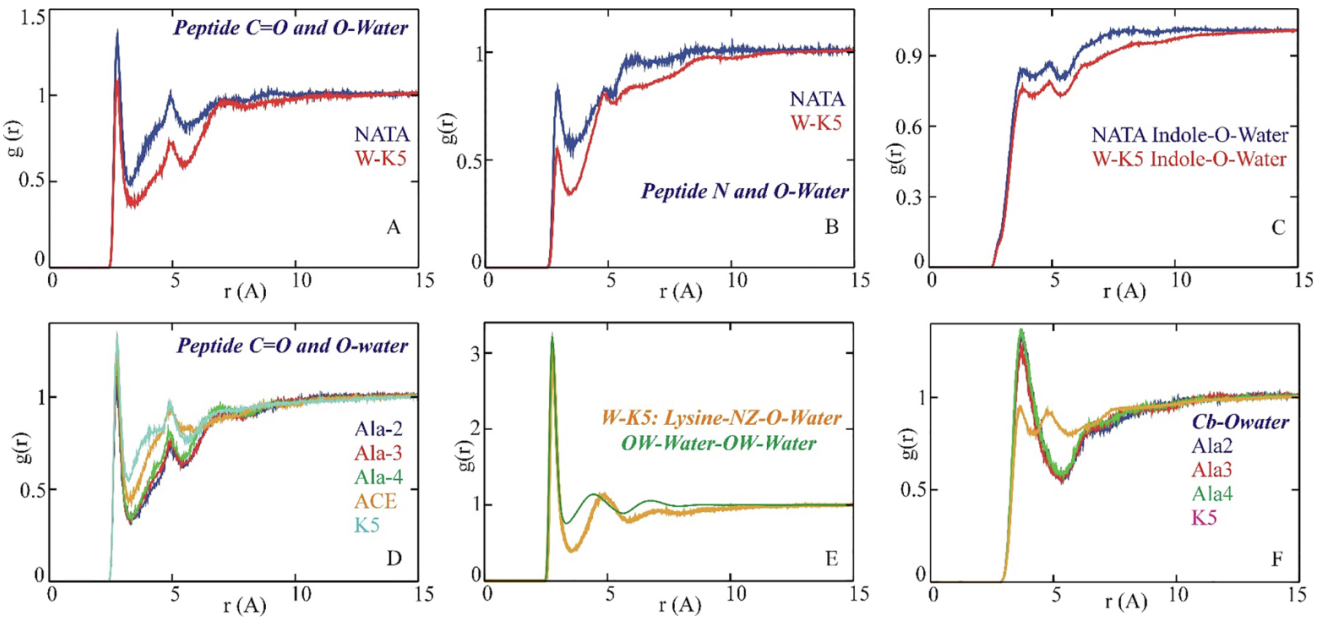

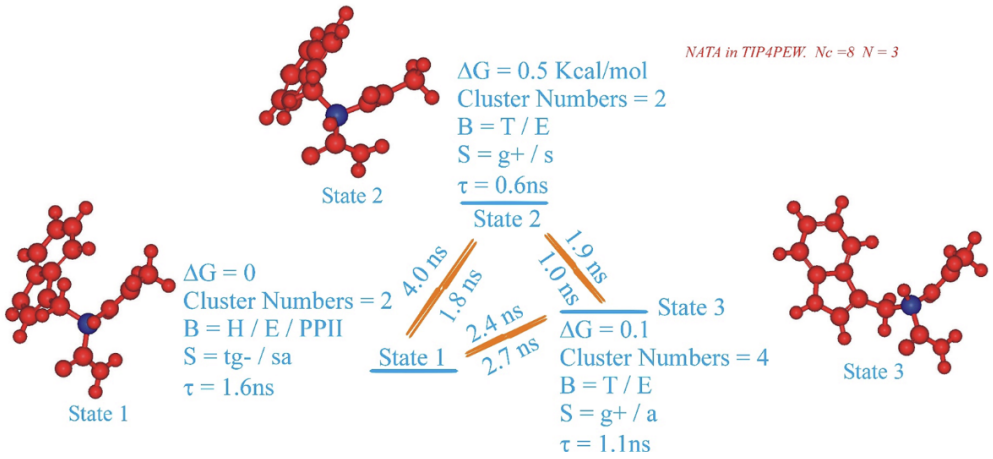

Fig. 11. Example kinetic model for NATA, based on discretization with $N_c = 8$ dihedral clusters and N = 3 coarse-grained states, showing state populations and ORD rates. B denotes backbone conformations (T – turn, E- extended, H – helix, PPII – polyproline II). S denotes sidechain conformations for χ_1(g+,g-,t) and χ_2 (a,s). State i lifetime τ is defined as $-1/R_{ii}$ and I to j transition time is $1/R_{ji}$, with R the ORD rate matrix.

on time scales of 7–19 ns. Typically, this relaxation is well separated from the remaining ones and the faster transitions are between different extended, PPII, and turn conformations. The TIP4P/EW results are in qualitative agreement with the earlier work involving the TIP4P water model with respect to sampled structures and associated time scales. However, there are differences in the details, since in TIP4P the 3_{10} helix state is more kinetically distinct, appearing as a mesostate even at the level of N = 2 coarse-grained states. As we increase the resolution to N = 3 and N = 4 states, the TIP4P and TIP4P/EW models become more similar. In this approach, the ORD and MSM models are found to be in qualitative agreement involving time scales and their state properties. For the largest number of clusters, the slowest MSM timescale is close to 19 ns, which is significantly longer than any relaxation process found in our analysis of comprehensive ACFs. Fig. 12 shows a sample kinetic analysis for WK5, with the trajectory discretization of Nc = 6 dihedral clusters and three coarse-grained states. The time scale associated with the dynamics is found to vary over a wide range, from tens of nanoseconds to single nanoseconds and faster. The importance of the 3_{10} helical state is demonstrated by this model.

4. Discussion

Peptides and proteins in solution are present in a perpetual motion. These motions include vibration, translation, rotation, and conformational transitions. In larger systems, like enzymes and multidomain proteins, it has been suggested that one part of the molecule initiates the motion, which then propagates across the entire molecule [10]. Based on the size and the structural complexity of a more flexible protein this initiation and propagation approach is reasonable. It is of fundamental interest to examine what would be the microscopic behavior of motion in solution upon initiation, in a substantially smaller system like the simplest dipeptide, NATA, and a model pentapeptide, WK5. Is it a prerequisite to have the presence of secondary, tertiary, and quaternary structures to constitute a coupled motion in solution for a biomolecule? If it is not a necessary condition, then how do these comparatively smaller biomolecular systems conduct their motion in an aqueous environment? To address these questions, we have constructed an atomically detailed picture of the reorientation dynamics of peptides in solution applying a set of complementary experimental and simulation studies.

Experimentally, we have performed FL, FAD, and CD analysis relative to temperature. Comprehensive all-atom MD of the solvated di- and pentapeptide were performed to generate an atomic level understanding of the experimental observables. Although near the instrument time resolution, the fastest measured time constant, ca. 6 ps for the simplest dipeptide NATA, is resolvable by our system. Reported longer

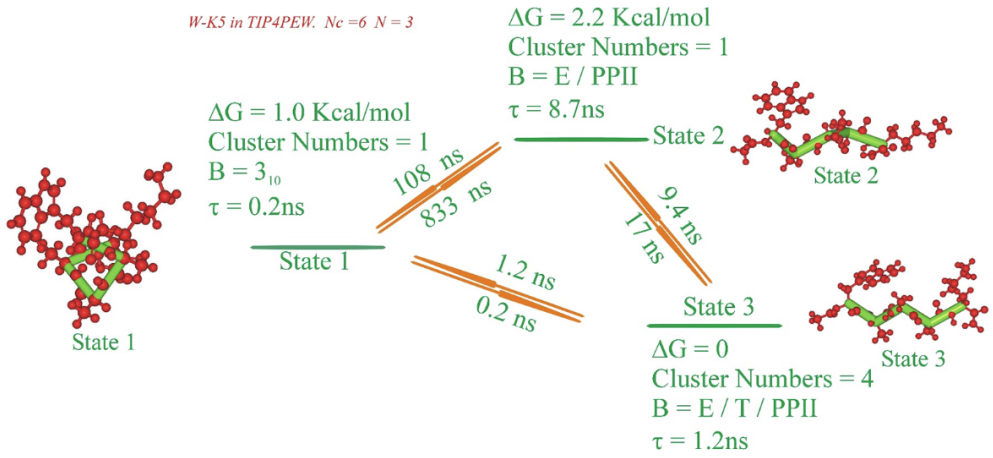

experimental time constants, between 28 ps and 250 ps, are well resolved under the current instrument set up.

CD measurements even in the simplest dipeptide like NATA showed a significant population of helix, beta, turn, and unordered structures at room temperature. In WK5, there is about 12% 3_{10} helix, as well as PPII, turn, unordered, and beta states at room temperature. The FL for both NATA and WK5 is getting shorter with increasing temperature, which is consistent with the intrinsic fluorescence property of tryptophan. Compared to NATA, WK5 fluorescence is quenched by Trp…Lys + interactions. Application of SVD to the temperature-dependent FL showed three distinct singular value amplitudes signifying the presence of three major populations for both NATA and WK5. This finding is consistent with the Far-UV CD analysis. Analysis of reorientation dynamics with FAD yielded two time-constants at each temperature for both peptides. The temperature-independent component of the time constants is most likely associated with the vibrational motion of the atoms upon excitation with photon energy. This exciting new find leads us to draw a pathway consisting of an initiation step with atomic vibrational motion following a propagated reorientation motion exploring the immediate solvent environment. This might be a clue to the mechanism of coupled motions observed in the reorientation dynamic of peptides in solution.

MD trajectories with TIP4P/EW explored, qualitatively, similar ranges of structures as found experimentally, including the 3_{10} helical state in WK5. MD identified three components of the solution peptide motion, ultrafast, in the sub-picosecond timescale, fast, in picoseconds, and slow in the nanosecond time domain. The origin of ultrafast and fast time constants may be assigned to localized and delocalized vibrations and the slowest to the conformational dynamics. Simulated peptide reorientation motions from MD analysis were in good agreement with the experiment. Experimentally observed temperature independent time scale associated motions were assigned to delocalized vibrations by MD simulation. The slower reorientation components were systematically faster than observed FAD data.

NORT trajectories indicated a significant coupling between internal fluctuations and global motions for these simplest peptide systems. This was confirmed by comparing the calculated structure factors S^2 from UNR and NORT MD. Differences between S^2 values calculated for NATA and WK5 were consistent with the presence of more stable structural elements and stronger coupling between internal and global dynamics in WK5 relative to NATA. solute–solvent interactions employing hydrogen bond lifetimes, SASA, van der Waals energy, and RDFs, present a clear structural difference between the two peptides. In NATA, the hydrogen bond lifetimes were shorter, SASA and energy fluctuations faster, and solvation of backbone peptide groups and the Trp sidechain by water oxygens stronger than in WK5. This may be due to the presence of compact stable structural elements and slower internal fluctuations in WK5. Based on the comprehensive analysis, we found that the atom groups and solvent molecules are the key component of the observed behavior in a reorientation dynamic.

Kinetic analysis applying ORD and MSM showed that the central feature of NATA kinetics involved sidechain transitions, with slowest processes in the 1 ns time scale. For WK5 the kinetics was in the 10 ns time scale and involved transitions between the 3_{10} helix and extended, turn, and PPII structures.

Here, combining carefully measured and comprehensively analyzed experimental data and extensive all-atom molecular dynamics simulation with the improved water model, divulge the presence of a coupled motion during global reorientation dynamics even in a simple system like a di- and a pentapeptide compared to a larger flexible molecule, like a protein in solution. Additionally, this study presented with an atomic-level description of the mechanism of the coupled motion observed in solution, suggesting an initiation, localized vibration, and then a propagation step, the global motion reorientation of the system.

Declaration of Competing Interest

The authors declare that they have no known competing financial interests or personal relationships that could have appeared to influence the work reported in this paper.

Acknowledgments

We would like to acknowledge XSEDE grant TG-MCB 16009 for computer time. Parts of the simulations described were conducted at the Center for Research Computing at the University of Kansas and on computer workstations supported by the General Research Fund at the University of Kansas. GSJ would like to thank Kyle Williams and Wade Burleson for helpful and inspirational discussion. GSJ would also like to thank Carey K. Johnson for the access to the fluorescence lifetime apparatus. This project was supported in part by an NSF grant CHE1807852.

Appendix A. Supplementary data

Supplementary data to this article can be found online at https://doi.org/10.1016/j.chemphys.2020.111018.

References.

[1] P.G. Wolynes, W.A. Eaton, Phys. World 12 (9) (1999) 39–44.
[2] J.D. Bryngelson, P.G. Wolynes, PNAS 84 (21) (1987) 7524–7528.
[3] R.F. Service, Science 321 (5890) (2008) 784–786.
[4] N. Go, Annu. Rev. Biophys. Bioeng. 12 (1983) 183–210.
[5] D. Voet, J. G. Voet, C.W. Pratt, p 154 (1999).
[6] K. Henzler-Wildman, K. Dill, Nature 450 (7172) (2007) 964–972.
[7] P.W. Fenimore, H. Frauenfelder, B.H. McMahon, P.G. Parak, Proc. Natl. Acad. Sci. U. S. A 99 (25) (2002) 16047–16051.
[8] H. van den Bedem, J.S. Fraser, Nat. Methods 12 (4) (2015) 307–318.
[9] H. Frauenfelder, P.W. Fenimore, R.D. Young, IUBMB Life 59 (8–9) (2007) 506–512.
[10] M.B. Hamaneh, L. Zhang, M.A. Buck, Biophys. J. 101 (1) (2011) 196–204.
[11] L. Makowski, D.J. Rodi, R.F. Fischetti, J. Mol. Biol. 375 (2) (2008) 529–546.
[12] C.J. Tsai, A. Del Sol, R. Nussinov, Mol. BioSyst. 5 (3) (2009) 207–216.
[13] Y. Wang, C. Li, G.J. Pielak, J. Am. Chem. Soc. 132 (27) (2010) 9392–9397.
[14] G.S. Jas, R. Vallejo, C.K. Johnson, K. Kuczera, J. Chem. Phys. 151 (22) (2019), 225102.
[15] H.W. Horn, W.C. Swope, J.W. Pitera, J.D. Madura, T.J. Dick, G.L. Hura, T. Head-Gordon, J. Chem. Phys. 120 (20) (2004) 9665–9678.
[16] G. Hummer, A. Szabo, J. Phys. Chem. B 119 (29) (2015) 9029–9037.
[17] G.S. Jas, K. Kuczera, J. Phys. Chem. B 122 (48) (2018) 10806–10816.
[18] G.R. Bowman, V.S. Pande, F. Noe, Eds., Springer, Dordrecht (2014).
[19] G.S. Jas, E.C. Rentchler, A.M. Słowicka, J.R. Hermansen, C.K. Johnson, C. R. Middaugh, K. Kuczera, J. Phys. Chem. B 120 (12) (2016) 3089–3099.
[20] G.S. Jas, W.A. Eaton, J. Hofrichter, J. Phys. Chem. B 105 (1) (2000) 261–272.
[21] W.A. Hegefeld, S.E. Chen, K.Y. DeLeon, K. Kuczera, G.S. Jas, J. Phys. Chem. A 114 (47) (2010) 12391–12402.
[22] O.F. Mohammed, G.S. Jas, M.M. Lin, A.H. Zewail, Angew. Chem. Int. Ed. Engl. 48 (31) (2009) 5628–5632.
[23] M.M. Lin, O.F. Mohammed, G.S. Jas, A.H. Zewail, Proc. Natl. Acad. Sci. U.S.A. 108 (40) (2011) 16622–16627.
[24] W.A. Hegefeld, K. Kuczera, G.S. Jas, Biopolymers 95 (7) (2011) 487–502.
[25] G.S. Jas, K. Kuczera, J. Phys. Chem. B 122 (49) (2018) 11508–11518.
[26] J. Hofrichter, J.H. Sommer, E.R. Henry, W.A. Eaton, Proc. Natl. Acad. Sci. U.S.A. 80 (8) (1983) 2235–2239.
[27] R.I. Shrager, R.W. Hendler, Anal. Chem. 54 (7) (1982) 1147–1152.
[28] G.H. Golub, C. Reinsch, Numer. Math. 14 (1970) 403–420.
[29] B.R. Brooks, C.L. Brooks, A.D. MacKerell, L. Nilsson, R.J. Petrella, B. Roux, Y. Won, G. Archontis, C. Bartels, S. Boresch, et al., J. Comput. Chem. 30 (10) (2009) 1545–1614.
[30] B. Hess, C. Kutzner, D. van der Spoel, E. Lindahl, J. Chem. Theory Comput. 4 (3) (2008) 435–447.
[31] G. Kaminski, W.L. Jorgensen, Phys. Chem. 100 (46) (1996) 18010–18013.
[32] P. Li, B.P. Roberts, D.K. Chakravorty, K.M. Merz Jr., Rational Design of Particle Mesh Ewald Compatible Lennard-Jones Parameters for +2 Metal Cations in Explicit Solvent, J. Chem. Theory Comput. 9 (6) (2013) 2733–2748.
[33] T.N. Heinz, W.F. Van Gunsteren, P.H. Hunenberger, J. Chem. Phys. 115 (3) (2001) 1125.
[34] D. Favro, Phys. Rev. 119 (1) (1960) 53–62.
[35] R.F. Steiner, Plenum Press, New York, 2, 1-51 (1991).

[39] M. Senne, B. Trendelkamp-Schroer, A.S.J.S. Mey, C. Schütte, F. Noe, J. Chem. Theory Comput. 8 (11) (2012) 2223–2238.
[40] P.R. Callis, B.K. Burgess, J. Phys. Chem. B 101 (46) (1997) 9429–9432.
[41] D. Toptygin, T.B. Woolf, L. Brand, J. Phys. Chem. B 114 (34) (2010) 11323–11337.
[42] C-P. Pan, P. L. Mui~no, M. D. Barkley, P. R. Callis, J. Phys. Chem. B 115(12), 3245–3253 (2011).
[43] S.P. Laptenok, N.V. Visser, R. Engel, A.H. Westphal, A. van Hoek, C.P.M. van Mierlo, I.H.M. van Stokkum, H. van Amerongen, A.J.W. Visser, Biochemistry 50 (17) (2011) 3441–3450.
[44] S.V. Kathuria, C. Kayatekin, R. Barrea, E. Kondrashkina, R. Graceffa, L. Guo, R. P. Nobrega, S. Chakravarthy, C.R. Matthews, T.C. Irving, O. Bilsel, J. Mol. Biol. 426 (9) (2014) 1980–1994.
[45] G.S. Jas, K. Kuczera, J. Phys. Chem. B 122 (49) (2018) 11508–11518.
[46] G.S. Jas, W.A. Hegefeld, C.R. Middaugh, C.K. Johnson, K. Kuczera, J. Phys. Chem. B 118 (26) (2014) 7233–7246.
[47] G.S. Jas, W.A. Hegefeld, P. Májek, K. Kuczera, R. Elber, J. Phys. Chem. B 116 (23) (2012) 6598–6610.
[48] A. Lobley, L. Whitmore, B.A. Wallace, Bioinformatics 18 (1) (2002) 211–212.
[49] K. Kuczera, J. Unruh, C.K. Johnson, G.S. Jas, J. Phys. Chem. A 114 (1) (2010) 133–142.
[50] E.B. Wilson Jr., J.C. Decius, P.C. Cross, Mc-Graw-Hill, New York, (1955).
[51] M. Wang, R.L. Schowen, R.T. Borchardt, K. Kuczera, Biochemistry 44 (19) (2005) 7228–7239.
[52] G. Lamm, A. Szabo, J. Chem. Phys. 85 (12) (1986) 7334–7348.
[53] S. Hayward, A. Kitao, F. Hirata, N. Go, J. Mol. Biol. 234 (4) (1993) 1207–1217.
[54] G. Lipari, A. Szabo, J. Am. Chem. Soc. 104 (17) (1982) 4546–4559.
[55] A. Luzar, D. Chandler, Nature 379 (6560) (1996) 55–57.